Eur. Phys. J. D **41**, 127–141 (2007)
DOI: 10.1140/epjd/e2006-00191-2

THE EUROPEAN PHYSICAL JOURNAL D

Structure and dynamics of cationic van-der-Waals clusters

II. Dynamics of protonated argon clusters

T. Ritschel[1], Ch. Zuhrt[1], L. Zülicke[1,a], and P.J. Kuntz[2]

[1] Universität Potsdam, Institut für Chemie, Karl-Liebknecht-Straße 24-25, 14476 Golm, Germany
[2] Hahn-Meitner-Institut, Abteilung SF5, Glienicker Straße 100, 14109 Berlin, Germany

Received 6 October 2005 / Received in final form 14 July 2006
Published online 18 August 2006 –

Abstract. A diatomics-in-molecules (DIM) model with ab-initio input data, which in part I successfully described the structure and bonding properties of protonated argon clusters Ar_nH^+, is used here to investigate some aspects of the dynamics of such aggregates for n up to 30. The simple triatomic ionic fragment, Ar_2H^+, is studied in some detail with respect to normal vibrations, characteristics of classical intramolecular dynamics as reflected in the Fourier spectra of dynamical variables, and accurate quantum states of the vibrational motion. For larger clusters Ar_nH^+ ($n \leq 30$), the normal vibrational frequencies (and displacement eigenvectors) are calculated and related to the cluster structure. In addition, the Fourier spectra are analyzed with respect to their variation with changing internal energy and cluster size. As expected, the clusters show some floppy character. Even a little vibrational excitation can lead to internal rearrangement and to Ar-atom evaporation from the clusters; this is studied in more detail for one small complex ($n = 3$). Electronic excitation to one of the low-lying excited states, which are all globally repulsive, leads to complete fragmentation (atomization) of the clusters. A variety of conceivable elementary collision processes involving protonated argon clusters are discussed. Some of these may play a role in the gas-phase formation of medium-sized Ar_nH^+ aggregates.

PACS. 36.40.Wa Charged clusters – 36.40.Qv Stability and fragmentation of clusters – 36.40.Jn Reactivity of clusters – 36.40.Mr Spectroscopy and geometrical structure of clusters – 34.30.+h Intramolecular energy transfer; intramolecular dynamics; dynamics of van der Waals molecules – 34.50.-s Scattering of atoms and molecules

1 Introduction

In the past two decades, cationic van-der-Waals clusters of the type Rg_nM^+, where Rg denotes a rare-gas atom and M some atom or small molecule, have attracted much attention (for an overview see, e.g., [1,2]). Theoretical research (on which we concentrate here) has mainly been focused on the bonding of such aggregates, on the corresponding structural properties in comparison to the neutral counterparts, and sometimes also on spectroscopic characteristics. Most of the studies consider the pure cationic rare-gas clusters Rg_n^+ with small and medium numbers of atoms, n. Much less is known about inhomogeneous systems containing an *impurity* M; only some work on protonated rare-gas complexes Rg_nH^+ with n up to 7, recent studies on $Ar_nH_3^+$ with n = 1–9, and a few papers on small complexes with diatomics M and $n = 1$ or 2 can be found in the literature. A compilation of references is given in our recent article (part I of this study) [3]. The dynamics of such aggregates is largely unexplored except for some work on a number of triatomic prototype complexes [4–7]. There is much less known about these clusters than for corresponding neutral systems [8].

Considering this situation, we have recently begun a systematic and extensive theoretical investigation of inhomogeneous cationic van-der-Waals clusters Rg_nM^+ with the following aims: (1) to enlarge the cluster size and look for the dependence of cluster properties on n, (2) to include also the low-lying excited electronic states, and (3) to gain some insight into the dynamical behaviour of such polyatomic aggregates. This is a task which requires, in particular, very efficient and at the same time sufficiently reliable computation procedures for all stages of the treatment.

In the first paper [3] of this series we reported on the binding and geometrical structure of protonated argon clusters, Ar_nH^+, a simple example of the inhomogeneous aggregates we are interested in. In the present article we extend this study to include the dynamics of such systems.

[a] e-mail: zuelicke@tc1.chem.uni-potsdam.de

Our method of approach is based on a minimum-basis diatomics-in-molecules (DIM) model for calculating the potential energy of interatomic interaction. This model is carefully parametrized with accurate ab-initio data as described in [3]. Using the potential-energy surface (PES) points generated, we investigate several aspects of the dynamical behaviour of small and medium-sized Ar_nH^+ cluster ions, namely intra-cluster dynamics as well as some collision processes involving the Ar_nH^+ species. The results should give insight into dynamical and spectroscopical properties, suggesting also how such aggregates could be prepared and spectroscopically detected.

The present paper is organized as follows: in Section 2 the problems to be treated are specified in more detail; in Section 3 the methodology is sketched along with a brief description of the peculiarities of the calculation procedures; Section 4 presents the results, first for the triatomic Ar_2H^+ complex, then for medium-sized clusters Ar_nH^+. Finally, in Section 5, we give a summary and an outlook.

2 The tasks

In the present study, we shall first consider those intramolecular motions which leave the overall cluster structure intact, i.e. the vibrations of the cluster. For triatomic complexes like Ar_2H^+, we are able to investigate the vibrations in great detail and with high precision in a quantum-mechanical approach. The vibrational quantum states can be accurately computed giving reliable data for zero-point and excitation energies and leading to conclusions about localization properties, floppy character, energy exchange between the modes, and possible irregularity of the intramolecular motion on the quantum level. These findings will be related to results of the normal-mode analysis and the classical-mechanical treatment, in particular the Fourier spectral analysis of classical trajectories, thus getting an idea of the reliability of the classical treatment and the harmonic approximation.

For the larger clusters, our study will be restricted to the classical level only, in order to avoid expensive quantum calculations which could, in principle, be carried out by means of iterative schemes like filter diagonalization (see, e.g., [9]). The classical approach should be able to describe at least the gross dependence of vibrational properties on the cluster size (n) and to reveal the possible onset of (classical) chaos.

Our second aim is to investigate some of those intracluster motions that are connected with the rearrangement of atoms within the cluster. We discuss two restructuring processes triggered by vibrational excitation, namely proton and argon-atom migration, and we consider also argon-atom detachment, all of these processes treated in a classical approach for one small sample cluster. This study does not claim completeness, in particular with respect to possible mode-specificity. Other related processes like structural relaxation will not be considered in detail. Furthermore, intra-cluster processes in excited electronic states as induced by ultraviolet or visible light irradiation will not be explicitly investigated since, due to the globally repulsive nature of the excited-state PESs, only complete fragmentation is to be expected, as already discussed in part I [3].

Thirdly, we examine at the classical level some selected elementary processes which may play a role in gaseous mixtures or in molecular beams: collisions involving neutral Ar atoms and clusters, protons and positively charged clusters. In particular, we consider neutral Ar_m clusters interacting with a proton,

$$H^+ + Ar_m, \tag{1}$$

and with a protonated argon cluster,

$$Ar_nH^+ + Ar_m. \tag{2}$$

It is not our aim to calculate cross-sections or reaction rate constants, but only to understand qualitatively what kinds of processes may occur; hence, we restrict the study to the analysis of some single, representative collision events. Also we do not aspire to completeness in this context; therefore, other conceivable and related processes like those between H atoms and pure cationic argon clusters, Ar_n^+, will not be considered.

3 Methodology

The basic approximation underlying our investigations is the adiabatic (Born-Oppenheimer) separation of electronic and nuclear degrees of freedom in its usually applied simplest version in which the potential-energy function governing the motion of the nuclei is given for each nuclear arrangement by the sum of the total energy of the electron cloud and the total electrostatic nuclear repulsion energy. Since relativistic effects do not play a role in the present case (in particular, there is no significant spin-orbit interaction), the first piece of work is the approximate solution of the nonrelativistic electronic Schrödinger equation for generating the interatomic-interaction potential energy as a function of the nuclear coordinates. This function can then be used in the nuclear Schrödinger equation or in the classical equations of nuclear motion governing the dynamics.

3.1 Potential-energy surface generation

The broad variety of applications envisaged in the present study puts demands upon the methods for generating the PES data: (i) it must be sufficiently reliable to give at least qualitatively correct interatomic-interaction potentials in dependence on the geometrical configuration of the nuclei, (ii) it should also admit the generation of interaction potentials for electronically excited states of the aggregates, and (iii) it must allow efficient calculation of each point on the multi-dimensional PESs. Because of the large number of variables $(3(n+1)-6$ nuclear degrees of freedom in the present case), an analytical fit of the total potential-energy

function is hardly practicable, so that there is no alternative to generating the PES points as they are needed (i.e., for example, "on the fly" in a trajectory propagation).

The only quantum-chemical approach which is able in practice to meet these requirements is the diatomics-in-molecules (DIM) model. For the systems studied here, the medium-sized protonated argon clusters, the fulfillment of demand (i) has been tested against advanced conventional ab-initio approaches in our foregoing papers [3,10]. Even the simplest version, the minimum-basis DIM model, is sufficient for our purposes.

We shall not describe the DIM model in detail but only summarize the main characteristics (we refer the reader to [3,10] and the literature citations therein):

- our DIM model for Ar_nH^+ takes into account all fragment states leading to singlet states of the whole cluster and lying energetically not more than about 10 eV above the respective fragment ground states:
  $Ar(^1S)$, $Ar^+(^2P^\circ)$, $H(^2S)$,
  $ArH(X^2\Sigma^+)$, $ArH^+(X^1\Sigma^+, 1^1\Pi, 2^1\Sigma^+)$,
  $Ar_2(X^1\Sigma_g^+)$, $Ar_2^+(X^2\Sigma_u^+, 1^2\Pi_g, 1^2\Pi_u, 1^2\Sigma_g^+)$.
  This "minimal DIM model" demands the smallest amount of fragment information consistent with a meaningful description of the clusters;
- the atomic and diatomic fragment data needed for the DIM procedure – namely: the atomic-state energies, the diatomic potential-energy functions and electronic wavefunctions in dependence on the internuclear distance – are very accurately determined by an internally contracted multi-reference configuration-interaction (icMRCI) approach including a generalized Davidson correction for the estimation of the energetic contributions of higher-order excitations (icMRCI + Q). For this task we used the MOLPRO program package [11].
  The set of one-electron atomic basis functions chosen for carrying out these calculations was the aug-cc-pVTZ basis set of Woon and Dunning [12] (containing also several diffuse functions), contracted to a total of $50n + 23$ basis functions;
- for converting the diatomic input data from the molecular-orbital (MO) based CI form, as obtained in the MRCI treatment, to a valence-bond (VB) form in which they are needed in the DIM ansatz, a projection procedure, elaborated by Kuntz and Schreiber [13], has been applied. If a mixing of VB configurations is required for a state considered (this is the case here for the two $^1\Sigma^+$ states of the fragment ArH^+), the projection onto a linear combination of the corresponding VB configurations is computed. The mixing coefficient is thus determined in a completely straightforward ab-initio-based way without any additional VB calculation.

This approach is what we name our "minimal ab-initio DIM model". It enables to calculate all the necessary PES data for the clusters Ar_nH^+ very efficiently on an equal footing. The topographical analysis of these data, in particular the determination of the local minima of the multi-dimensional PESs has been discussed in part I of this series; here, in part II, the PES points are used as input to the methods for studying the dynamical properties of the clusters.

3.2 Vibrations and intra-cluster processes

The intramolecular vibrational motions of a polyatomic aggregate can be most easily described by the model of normal vibrations as long as the harmonic approximation to the PES in the neighbourhood of the local minima is sufficient, i.e. as long as the minima are deep enough, separated by high barriers, and the vibrations are of small amplitude. If this is not the case, i.e. the minima of the PES are flat with low barriers between them, and the nuclear motions have large amplitudes, then the harmonic approximation breaks down, the modes are strongly coupled, and the whole aggregate shows what is often called *floppy* character. For triatomic systems this behaviour has been rather intensively studied (see, e.g., [14]) within the framework of classical as well as quantum-mechanical approaches; this will also be done here for the triatomic fragment Ar_2H^+.

For larger clusters Ar_nH^+ the task of studying the internal dynamics is much more difficult, even with good PES data available; in particular, a quantum-mechanical treatment is connected with serious problems so that one usually resorts to traditional classical tools.

3.2.1 Quantum-mechanical treatment of the Ar_2H^+ triatomic fragment vibrations

The treatment of vibrating triatomic molecules is nowadays essentially a routine task using, e.g., the truncation recoupling method [15] or filter diagonalization [9]. Nevertheless, although the computation methodology is well established, such calculations may not always be trivial, especially for floppy molecules and special mass combinations of the atoms involved. In the case of Ar_2H^+ it turns out to be difficult to find an appropriate and computationally efficient coordinate system. After some attempts with Radau coordinates [16] (which proved ill-suited because of the light central atom) and several solution methods for the Schrödinger equation we finally decided to employ the procedure outlined below.

After separating the center-of-mass motion and introducing symmetric atom-diatom Jacobi coordinates (namely the Ar–Ar internuclear distance r, the distance R from the Ar_2 center of mass to H, and the Jacobi angle θ enclosed by the vectors $\boldsymbol{r}$ and $\boldsymbol{R}$), a factor $(1/rR)$ is usually split off from the complete wavefunction $\Psi(r, R, \theta)$:

$$\Psi(r, R, \theta) = \frac{1}{rR}\Phi(r, R, \theta). \tag{3}$$

This entails no loss of information and is done for mathematical simplicity. Of course, the step is accompanied with a change in the volume element from $r^2R^2\mathrm{d}r\mathrm{d}R\sin(\theta)\mathrm{d}\theta$ (in connection with Ψ) to $\mathrm{d}r\mathrm{d}R\sin(\theta)\mathrm{d}\theta$ (for Φ). For the vibrational states of the triatomic molecular system with

zero total angular momentum ($J = 0$), the transformed wavefunctions $\Phi(r, R, \theta)$ are the normalized solutions of the time-independent Schrödinger equation

$$\hat{H}\Phi(r, R, \theta) = E\Phi(r, R, \theta) \tag{4}$$

with the Hamiltonian given by

$$\hat{H} = -\frac{\hbar^2}{2\mu}\frac{\partial^2}{\partial r^2} - \frac{\hbar^2}{2M}\frac{\partial^2}{\partial R^2} - \frac{\hbar^2}{2}\left(\frac{1}{\mu r^2} + \frac{1}{MR^2}\right)\frac{1}{\sin(\theta)}\frac{\partial}{\partial\theta}\sin(\theta)\frac{\partial}{\partial\theta} + V(r, R, \theta) \tag{5}$$

where μ and M are the appropriate reduced masses of the particle pairs Ar–Ar and H–Ar_2, respectively.

In order to guarantee that the complete vibrational wavefunctions Ψ will not become singular at $R = 0$, the functions Φ have to obey, among others, the boundary condition $\lim_{R\to 0}\Phi(r, R, \theta) = 0$.

The symmetric Jacobi coordinates have two disadvantages: (i) they lead to a singularity in the Hamiltonian at $R = 0$, which lies in the classically accessible region, and (ii) they do not lend themselves well to the separation of the vibrational motion; this hampers the interpretation of the results. Nevertheless, these undesirable features do not preclude meaningful calculations.

For the solution of the vibrational bound-state problem we use a discretization within the discrete variable representation (DVR) with sinc basis functions [17] for the two distance coordinates r, R, and Legendre polynomials for the angular basis:

- for the r coordinate 100 points in the range $[4.6, 9.0]$ a_0,
- for the R coordinate 100 points in the range $[0.05, 5.4]$ a_0,
- for the θ coordinate 50 points, reduced to 25 by symmetry.

Despite the relatively large extension of this grid, the range of vibrational states that can be reasonably described is limited to energies up to the saddle point at about 0.4 eV; this is due to the boundary conditions.

The Schrödinger equation was solved both for gerade and ungerade symmetry by an improved filter diagonalization method [9,18] using filter basis functions constructed from 50,000 Chebyshev polynomials.

3.2.2 Classical intra-cluster dynamics

The most obvious approach to the internal dynamics of a cluster (which can even be directly visualized) is the normal-mode model. It is obtained largely as a by-product of the topographical analysis of the PES, namely from the diagonalization of the Hessian matrix (second derivatives of the potential-energy function) at the stationary point considered. This procedure in either analytical, numerical, or mixed form is standard and is included in most of the program packages; more explanation is therefore hardly necessary here (see, e.g., [19]).

Some detailed information about the classical dynamics of the nuclear motion in dependence on the initial conditions (in particular on the initial internal energy) and on the cluster size (n) can be gained from a Fourier analysis of appropriate dynamical variables $Z(t)$ as functions of time t (e.g., coordinates as the simplest choice). This means that the *spectral density* (*power spectrum*),

$$I(\omega) = \lim_{T\to\infty}\left\langle \frac{1}{2T}\left|\int_{-T}^{T} Z(t)\exp(-i\omega t)dt\right|^2\right\rangle, \tag{6}$$

has to be computed; here the brackets $\langle\,\rangle$ indicate an ensemble average over the initial vibrational phases of the trajectories in a batch. The observation time, $2T$, over which the trajectories are followed, was some 30 ps; the sampling interval, spectral resolution, and critical frequency were chosen appropriately in each case in order to obtain reliable spectra.

Usually, the feasibility of intra-cluster rearrangement processes is determined largely by the shape of the PES along the reaction path (minimum-energy path) connecting the two local minima corresponding to the reactant and product structures via a saddle point transition configuration. The dynamics of the processes is described here by classical trajectories. Again this is a standard procedure so that further detailed explanation is not necessary; we note only: the classical Hamiltonian equations of motion are formulated in terms of Cartesian coordinates of all the atoms involved [20]. After selecting the complete set of appropriate initial conditions the integration of the equations of motion is accomplished by using a combined fourth-order Runge-Kutta, fifth-order Adams-Bashforth-Moulton algorithm [21]. The integration is started by executing five cycles of Runge-Kutta integration with a fixed time step Δt for preparing a table of coordinates and momenta at the first five multiples of Δt. This table is then used to continue the integration by the more efficient Adams-Bashforth-Moulton method. Although the latter allows for the use of variable time steps, we have chosen a uniform time step Δt in order to be able to perform an FFT analysis of the trajectory data. Depending on the system size, time steps of $\Delta t = 5\times 10^{-17}$–$5\times 10^{-15}$ s are used throughout.

We mention here as an alternative approach to the whole problem of cluster dynamics the Car-Parrinello method [22], which is based on the density-functional theory for the description of the electrons and, up to now, restricted to the electronic ground state. Therefore it was not considered in our project; however, for problems maintaining the electron cloud in its ground state a comparison with our results would be of interest.

3.3 Collisions involving clusters

Because of the large number of degrees of freedom, we also use the classical trajectory approach (as described above) for the treatment of collisions of clusters with other particles (atoms, molecules, or clusters). This requires some preparatory work over and above the standard procedure

Table 1. DIM geometry data, binding (atomization) energies, atomic charges, harmonic frequencies, and zero-point energies (ZPE) for the stationary points of Ar_2H^+, Ar_2^+, and ArH^+.

			Geometry[b]			Atomic charges			Harmonic frequencies[c]			
		E_B [a]	r_1	r_2	α	q_1	q_2	q_H	ω_1	$\omega_{2,3}$	ω_4	ZPE
		eV	a_0	a_0	deg	a.u.	a.u.	a.u.	cm^{-1}	cm^{-1}	cm^{-1}	eV
(a)	Ar_2H^+ ($1^1A'$)											
	Min 1 ($D_{\infty h}$)	−4.566	2.76	2.76	180.0	0.182	0.182	0.635	1157	592	306	0.164
	Min 2 ($C_{\infty h}$)	−4.184	8.90	2.42	0.0	0.001	0.366	0.633	2736	42	56	0.178
	SP (C_s)	−4.182	8.49	2.42	31.5	0.001	0.365	0.634	2740	51i	56	0.173
(b)	Ar_2^+ ($X^2\Sigma_u^+$)	−1.322	4.58			0.500	0.500				300	0.019
(c)	ArH^+ ($X^1\Sigma^+$)	−4.132	2.42			0.364		0.636	2737			0.170

[a] Binding energy E_B: total energy relative to the sum of the energies of the separated ground-state atoms or ions: $Ar(^1S)$, $Ar^+(^2P^\circ)$, and H^+, respectively, for the three cases (a), (b), and (c) considered.
[b] r_1 and r_2 are the distances of the proton H^+ from the first and the second Ar nucleus, $Ar^{(1)}$ and $Ar^{(2)}$, respectively, in Ar_2H^+. For Ar_2^+, r_1 denotes the Ar–Ar distance. α is the angle $\angle Ar^{(1)}HAr^{(2)}$.
[c] The numbering of the normal vibrations is: 1 – asymmetric stretch, 2, 3 – bend, 4 – symmetric stretch. For the (nonlinear) saddle-point configuration there is only one bending vibration.

with regard to the choice of the initial conditions, which are specified as follows: first the reacting partners are separated to very large distances (≈1000 a_0) in order to prepare their initial vibrational states, chosen to have random vibrational phases. Then the partners are brought to a shorter distance (typically 25–30 a_0), the translational momentum vectors are added according to the selected impact parameter and the translational energy, and the integration of the equations of motion is started. All calculations have been performed for non-rotating collision partners.

4 Results and discussion

4.1 Normal vibrations, vibrational quantum states, and internal dynamics of the Ar_2H^+ complex in its electronic ground state

Among the interesting topics in the context of the present study is the reliability of the harmonic approximation and the classical-mechanical approach. The strongly bound linear centro-symmetric complex $(Ar–H–Ar)^+$ plays the role of a chromophore of the Ar_nH^+ clusters in their most stable geometric configurations, as discussed in part I [3], so that it is highly desirable to know its vibrational-state properties as accurately as possible.

4.1.1 DIM ground-state PES characteristics

For the above-mentioned complex, the ground-state PES has been calculated in the minimum-basis ab-initio DIM approach in part I of this series [3], briefly summarized also in [10]. We describe the topography of the PES for the electronic ground state of the Ar_2H^+ complex by the internal coordinates r_1, r_2, and α as defined in footnote *b* to Table 1 where the relevant energetic and geometric data as well as atomic charges and harmonic frequencies for the stationary points are given. In Figure 1 a two-dimensional plot of the DIM potential-energy function $U(r_1, \alpha)$ for Ar_2H^+ with r_2 fixed is shown.

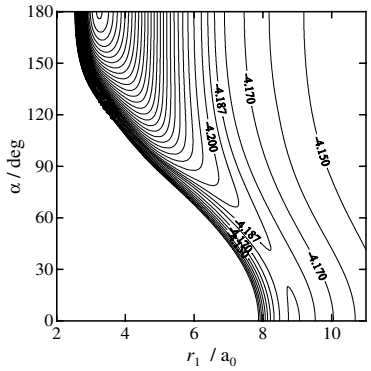

Fig. 1. Potential-energy contour-line diagram for the Ar_2H^+ electronic ground state ($1^1A'$) as obtained with the DIM model: $U(r_1, \alpha)$ with $r_2 = 2.42$ a_0 fixed. The energy values are given relative to the separated-atom limit $2Ar(^1S) + H^+$.

The most stable structure of Ar_2H^+ (Min1, global minimum of the ground-state PES) is the above-mentioned firmly bound linear centro-symmetric $(Ar–H–Ar)^+$ complex. There is a second local minimum (Min2) corresponding to an ArH^+ molecular ion, loosely bound to an Ar atom in a linear $Ar\cdots ArH^+$ complex. The two minima are separated by a saddle point (SP), see Figure 1. These topographical features (compare [3,10]) agree well with results of other authors (see, e.g., [23]).

4.1.2 Analysis of classical Ar_2H^+ dynamics

Our first step towards the dynamics is the inspection of the normal vibrations of the Ar_2H^+ complex in its most stable structure corresponding to Min1. The displacement vectors for the four normal vibrations of the linear centro-symmetric complex are shown in Figure 2. These pictures and the gradation of frequencies are easily understood: the slowest is the symmetric heavy-atom (Ar–Ar) stretching vibration, somewhat faster is the (twofold degenerate)

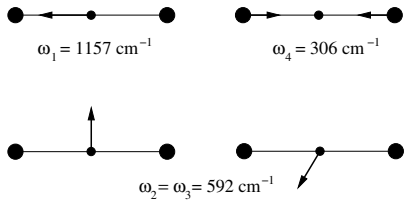

Fig. 2. Normal vibrations of the linear Ar_2H^+ complex (Min1): frequencies and displacement vectors.

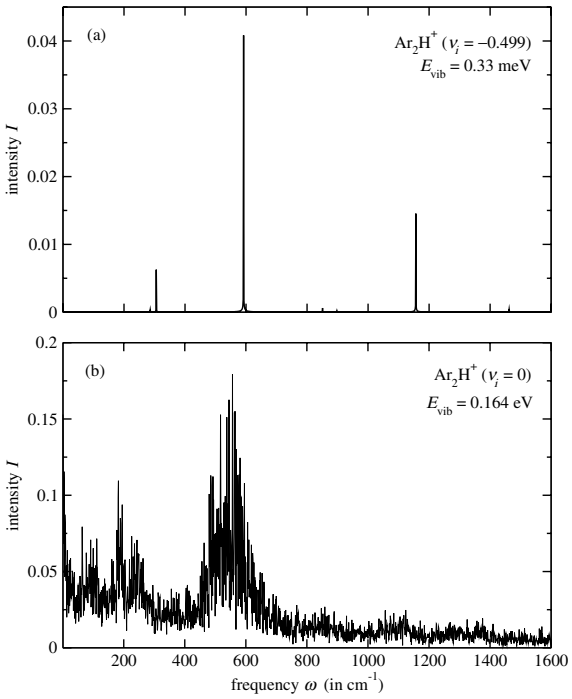

Fig. 3. Fourier spectrum of the superposition of all Cartesian coordinates for classical vibrational motion of the linear Ar_2H^+ complex (Min1); initial conditions corresponding to normal-mode vibrations: (a) $\nu_i = -0.499$; (b) $\nu_i = 0$.

bending, and much faster is the asymmetric stretch involving mainly the proton as the lightest particle of the system. From the symmetry properties at Min1, coupling is expected to be strongest between the two σ modes, symmetric and asymmetric stretching. This qualitative conjecture is verified by inspection of Figure 3 which shows, for two values of the vibrational energy, the Fourier spectrum, according to equation (6), of the classical vibrational motion of the linear centro-symmetric complex (Min1). The dynamical variable $Z(t)$ is taken as the superposition of all Cartesian coordinates of the nuclei, which guarantees that all frequencies occurring will also appear in the spectrum. For very low vibrational energy (so to speak: "sub-zero-point" vibration, $\nu_1 = \nu_2 = \nu_3 = \nu_4 = -0.499$, which is allowed in the classical approach) we see a clean line spectrum of the normal frequencies with indications of a few combination and overtone frequencies. Such a spectrum is typical for largely regular dynamics. With elevated energy, anharmonicity comes quickly into play, the modes get more and more strongly coupled and the spectrum exhibits increasingly noisy character, pointing to irregular, chaotic classical dynamics. As can be seen from Figure 3, in the case considered we are already in the classically chaotic regime even for a vibrational energy as low as the zero-point energy. The classical dynamics remains chaotic also for higher vibrational energies. Thus we find here for the triatomic Ar_2H^+ complex the same sort of behaviour of the classical vibrational motion – the early onset of irregularity because of the PES anharmonicity and mode coupling – as in other systems of this kind (see, e.g., [5,7]).

4.1.3 Vibrational quantum states of Ar_2H^+ ($J = 0$)

With the procedure outlined in the Section 3.2.1 the vibrational spectrum for $J = 0$ of the electronic ground state of Ar_2H^+ was calculated up to an energy of 0.43 eV, slightly below the first dissociation threshold, with an estimated accuracy of about 0.1 cm^{-1}; of course, this refers only to the accuracy of the solution of the vibrational problem for the DIM PES employed, the errors of which are several orders of magnitude larger. Furthermore it should be mentioned that the highest states should probably have additional errors due to the limited size of the grid with respect to the distance coordinates r, R. We are fully aware that the results therefore are to be considered as only qualitatively correct. Nevertheless it seemed to be reasonable to treat all parts of the problem as accurately as we could with our present means, thus providing reference data for comparing methods.

The calculation resulted in 19 vibrational states for the *gerade* symmetry and 12 for the *ungerade* symmetry which are listed in Table 2 together with a tentative assignment of quantum numbers. Because of the highly inseparable nature of the vibrational Hamiltonian in the coordinates employed, the designation of states by quantum numbers is not always obvious and sometimes questionable. By analysis of the wavefunctions and additional information from various expectation values of energetic and geometrical quantities an unequivocal assignment turned out to be possible in most cases. Representative examples of contour plots for the r, R dependence of the wavefunctions $\Phi(r, R, \theta)$ are given in Figures 4 and 5. To understand these pictures the following should be noted. Due to the transformation (3), in the limit $R \to 0$ the wavefunctions for the states $(0, x, y)$ behave as $\Phi \sim R$, while for the states $(1, x, y)$ we have $\Phi \sim R^2$. Consequently the absolute values of the complete wavefunctions Ψ for the states $(0, x, y)$ tend to a maximum for $R \to 0$, and for the states $(1, x, y)$ their limiting behaviour is $\Psi \sim R$.

For the *gerade* vibrational states (Σ_g^+ species) in Table 2a we have mainly two families of progressions $(0, x, y)$ of the Ar–Ar symmetric stretch vibration (y) in the ground state $(x = 0^0)$ and the excited state $x = 2^0$ of the bending vibration. These progressions exhibit strong anharmonicities and also some irregularities due to Fermi resonances for the *gerade* states 15–18. The assessment for the *gerade* state 18 is less clear as reflected also in the corresponding wavefunction plot, see Figure 4b; this is

Table 2. Vibrational eigenvalues and assessment of states for the electronic ground state of Ar_2H^+, calculated with the restriction $J = 0$.

(a) *gerade* states (Σ_g^+)

i	assignment[a]	E^{vib} [b]
1	(0, 0^0, 0)	1323
2	(0, 0^0, 1)	1586
3	(0, 0^0, 2)	1841
4	(0, 0^0, 3)	2086
5	(0, 0^0, 4)	2315
6	(0, 2^0, 0)	2482
7	(0, 0^0, 5)	2523
8	(0, 0^0, 6)	2704
9	(0, 2^0, 1)	2719
10	(0, 0^0, 7)	2866
11	(0, 2^0, 2)	2927
12	(0, 0^0, 8)	3012
13	(0, 2^0, 3)	3103
14	(0, 0^0, 9)	3149
15	(0, 2^0, 4)	3260
16	(0, 0^0, 10)	3282
17	(0, 0^0, 11)	3390
18	(0, 2^0, 5)	3409
19	(2, 0^0, 0)	3468

(b) *ungerade* states (Σ_u^+)

i	assignment[a]	E^{vib} [b]
1	(1, 0^0, 0)	2246
2	(1, 0^0, 1)	2437
3	(1, 0^0, 2)	2613
4	(1, 0^0, 3)	2776
5	(1, 0^0, 4)	2925
6	(1, 0^0, 5)	3064
7	(1, 2^0, 0)	3093
8	(1, 0^0, 6)	3195
9	(1, 2^0, 1)	3240
10	(1, 0^0, 7)	3319
11	(1, 2^0, 2)	3374
12	(1, 0^0, 8)	3438

[a] The numbering of the modes is the same as in the foregoing text and in Table 1, twofold degeneracy of the bend mode included and vibrational angular momentum quantum number as upper index indicated.
[b] The vibrational energy (in cm^{-1}) is measured relative to the bottom of the potential-energy well for Min1 (see Tab. 1).

an indication, that the coordinates employed are not well suited for revealing the node patterns of the wavefunctions in the (r, R) coordinate plane (which is also the case for the other two-dimensional projections in Jacobi coordinates). The highest state obtained (no. 19 in Tab. 2a), is the only one with two quanta in the asymmetric stretch vibration.

The *ungerade* vibrational states (Σ_u^+ species) in Table 2b show a very similar behaviour: they start with the first asymmetric stretch state $(1, 0^0, 0)$, and we have again two families of progressions $(1, x, y)$ of the Ar-Ar symmetric stretch vibration (y): for the bending vibration in the ground state $(x = 0^0)$ and in the excited state $x = 2^0$. The quanta of the symmetric stretch vibration are somewhat smaller than in the *gerade* case, which is just a consequence of the change in geometry and the increasing anharmonicity for higher vibrational energies. Also here the examples of vibrational-wavefunction contour plots in Figure 5 are more or less self-explanatory and show a rather clear and typical pattern for all vibrational states.

These findings altogether lead to the conclusion that the quantum dynamics of the triatomic complex does not show any indication of irregularity ("quantum chaos", for example in the nodal structure of the wavefunctions) – whereas classical dynamics does, as seen above.

Concerning the validity of the harmonic approximation, we observe that it gives the zero-point energy very accurately: 0.164 eV (see Tab. 1), in agreement with the quantum-mechanical calculation (see the state $(0, 0^0, 0)$ in Tab. 2a) which uses the complete anharmonic DIM PES. This supports the discussions concerning the cluster stability in part I [3]. A more detailed comparison of the quantum-mechanical data given in Table 2 (restricted to $J = 0$ but taking into account the full anharmonicity) with the results of the harmonic approximation is possible if we consider the vibrational energy level differences. The lowest excitation frequency for the asymmetric stretch vibration, $\Delta\omega(00^00 \rightarrow 10^00) = 923\ cm^{-1}$, is substantially smaller than the harmonic frequency $\omega_1 = 1157\ cm^{-1}$. However, the second excitation quantum, $\Delta\omega(10^00 \rightarrow 20^00) = 1222\ cm^{-1}$, is larger than the harmonic level spacing ω_1. Thus we take note of a strong anharmonicity of the asymmetric stretch vibration. For the symmetric stretch, the anharmonicity is also significant as can be seen from the discrepancy of the quantum $\Delta\omega(00^00 \rightarrow 00^01) = 263\ cm^{-1}$ vs. $\omega_4 = 306\ cm^{-1}$; for the higher excitations of this mode the deviations increase even more. The only excitations from our quantum-mechanical calculations, which can be assigned to the bending vibration, are the two-quantum transitions $(x = 0^0 \rightarrow 2^0)$, e.g. the lowest one, $\Delta\omega(00^00 \rightarrow 02^00) = 1159\ cm^{-1}$. This value is in surprisingly good agreement with $2\omega_{2,3} = 1184\ cm^{-1}$. But already for somewhat higher excited molecular vibrational states (with increasing y, e.g.) the transition frequencies quickly deviate more from $2\omega_{2,3}$, thus indicating strong anharmonicity also in the bending normal mode.

4.2 Normal vibrations and internal dynamics of Ar_nH^+ clusters with $n > 2$

For the medium-sized protonated argon clusters Ar_nH^+ with $n > 2$, we confine our study to the classical approach. Encouragement for doing so can be taken from the calculations of the vibrational quantum states of the triatomic complex Ar_2H^+ (*vide supra*), which show that, at least for the low-energy regime (in particular for the zero-point motion), the normal-mode approximation and the classical trajectory treatment should give qualitatively correct answers also to questions about the general behaviour of the dependence of vibrational motion on the cluster size (n), except for the problem of irregularity.

Having this in mind, we computed the normal-mode frequencies and eigenvectors of all Ar_nH^+ aggregates with n = 2–30, each for the most stable structure of their electronic ground states as determined in the DIM treatment [3]. In Table 3 the normal frequencies for the smallest complexes with n = 2–8 are collected, and Figure 6 shows graphs of the dependence of the normal frequencies on n. What one realizes from these data is the following: (1) for each cluster (n) the frequencies can be grouped into two sets. The first set consists of four frequencies, which are clearly attributed to the four normal vibrations of the (always nearly linear) triatomic central fragment Ar_2H^+ embedded in a more or less symmetric environment of surrounding Ar atoms. One frequency around 1100 cm^{-1} is easily recognized as belonging to the asymmetric stretch

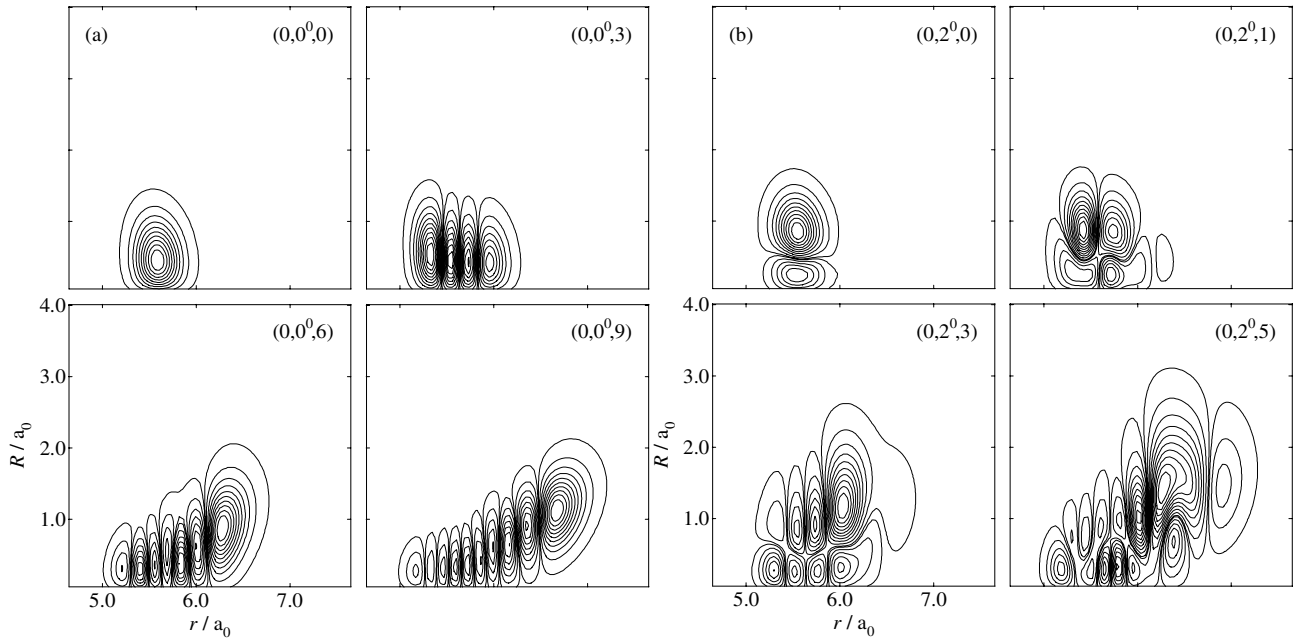

Fig. 4. Examples of contour maps of the *gerade* vibrational wavefunctions Φ in dependence on the Jacobi coordinates R and r for the progression of states (a) (0, 0^0, y) , (b) (0, 2^0, y). The coordinate θ is always fixed to the most probable value for the respective state.

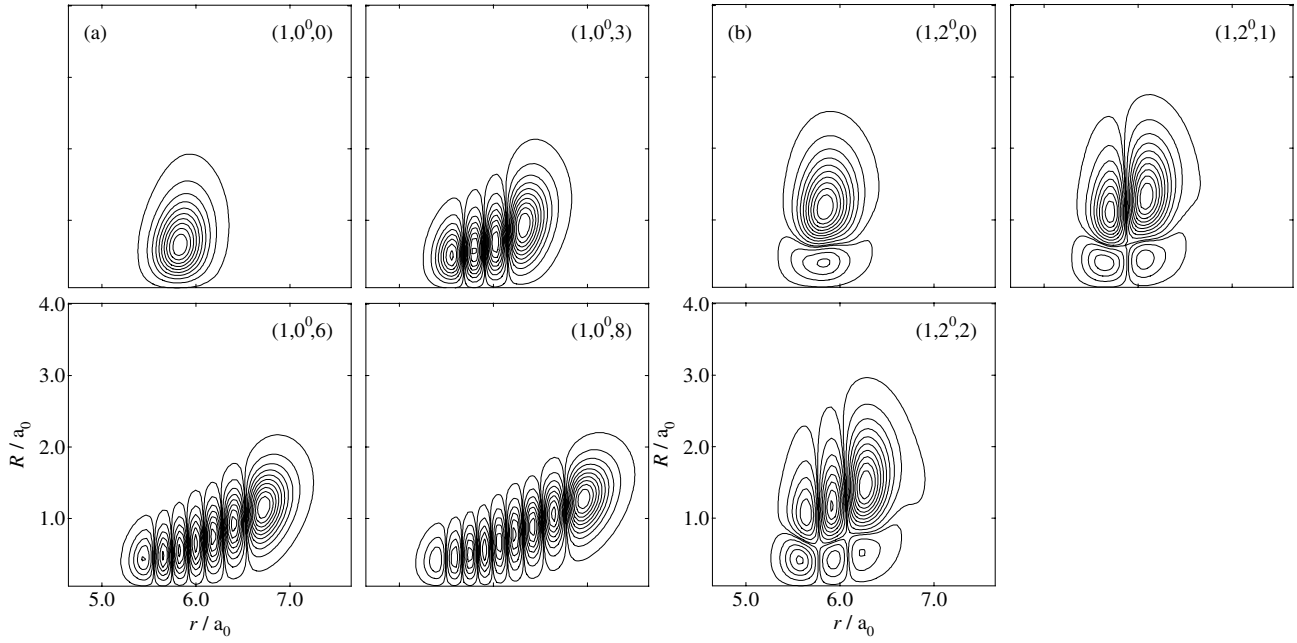

Fig. 5. Examples of contour maps of the *ungerade* vibrational wavefunctions Φ in dependence on the Jacobi coordinates R and r for the progression of states (a) (1, 0^0, y) , (b) (1, 2^0, y). The coordinate θ is always fixed to the most probable value for the respective state.

vibration of the Ar_2H^+ core fragment (essentially the oscillation of the proton between the two heavy Ar atoms). The next lower two frequencies correspond to the bending motion of the core fragment; this pair of frequencies becomes degenerate in the highly symmetrical clusters with $n = 2$, $n = 7$ (first closed ring) etc. but splits in the unsymmetrical structures, always remaining between 500 and 600 cm^{-1}. The fourth frequency, roughly 300 cm^{-1}, comes from the symmetric stretch vibration of the Ar atoms in the core fragment. All the other normal frequencies form the second set appearing from $n = 3$ on; they belong to the vibrations of the weakly bound extra-core Ar atoms and have correspondingly small values, below 100 cm^{-1} in the range of n considered. Clearly, one might distinguish here several subsets, which could be attributed to different vibrational modes of these outer Ar atoms. (2) The

Table 3. Normal frequencies of Ar_nH^+ with n = 2–8, and corresponding zero-point energies (all in cm^{-1}).

Ar_2H^+	Ar_3H^+	Ar_4H^+	Ar_5H^+	Ar_6H^+	Ar_7H^+	Ar_8H^+
1157.3	1134.6	1106.2	1095.7	1093.5	1092.9	1098.5
591.8	598.9	577.1	575.6	558.8	529.5	529.0
591.8	562.7	567.8	540.4	524.7	529.5	527.9
305.9	303.1	299.4	299.4	300.9	302.0	301.1
	52.8	57.7	57.6	61.7	60.4	67.0
	48.3	55.3	57.2	61.1	60.4	61.3
		51.5	55.1	56.9	60.2	60.7
		40.7	54.1	54.2	60.2	60.2
		24.3	43.3	45.6	48.2	48.4
			29.5	43.1	43.0	43.8
			27.1	36.2	43.0	43.5
			19.5	29.4	41.8	43.0
				24.3	32.2	37.9
				23.6	32.2	33.6
				13.7	25.1	32.1
					25.1	30.6
					22.2	28.4
					22.2	25.4
						22.1
						18.0
						13.4
1323.4	1350.2	1390.0	1427.3	1463.8	1515.1	1562.9

frequencies within each set depend in a characteristic way on the cluster size, obviously related to the structure of the cluster, as seen in Figure 6. For the medium-sized clusters considered here, the building-up of the most stable structures (according to Fig. 6 of part I [3]) is accompanied by marked changes in the four core vibrational frequencies up to $n = 19$. Starting from Ar_2H^+, the formation of the central five-membered Ar ring leads to a decrease of asymmetric stretch and the bending frequencies of the core (which are now non-degenerate), whereas the symmetric stretch vibration is almost unaffected. When the following, extra-central Ar ring is successively filled up plus the cap Ar atom added (n = 8–13), the frequencies change quite differently, such that now the bending vibration is not influenced very much (slightly decreasing), while the two stretch modes depend strongly on n, in opposite directions: the asymmetric stretch frequency increases and the symmetric stretch frequency decreases. On formation of the next five-membered Ar ring plus cap Ar atom on the other side, the stretch modes change their frequencies again: the asymmetric stretch vibration becomes slower and symmetric stretch faster, up to $n = 19$. For the most unsymmetrical cluster, that with $n = 13$, the asymmetric stretch frequency reaches its maximum value, the symmetric stretch its minimum. Beyond $n = 19$, when outer (secondary) Ar shells are being built up, the core normal frequencies do not change so markedly any more; this is what one would expect. The asymmetric stretch frequency slowly decreases, reflecting stepwise the magic numbers; we speculate that for larger clusters ($n > 30$) the curve will flatten out somewhere around 1000 cm^{-1}. Also for the other two core fragment modes the frequencies will level off as can be presumed from the curves.

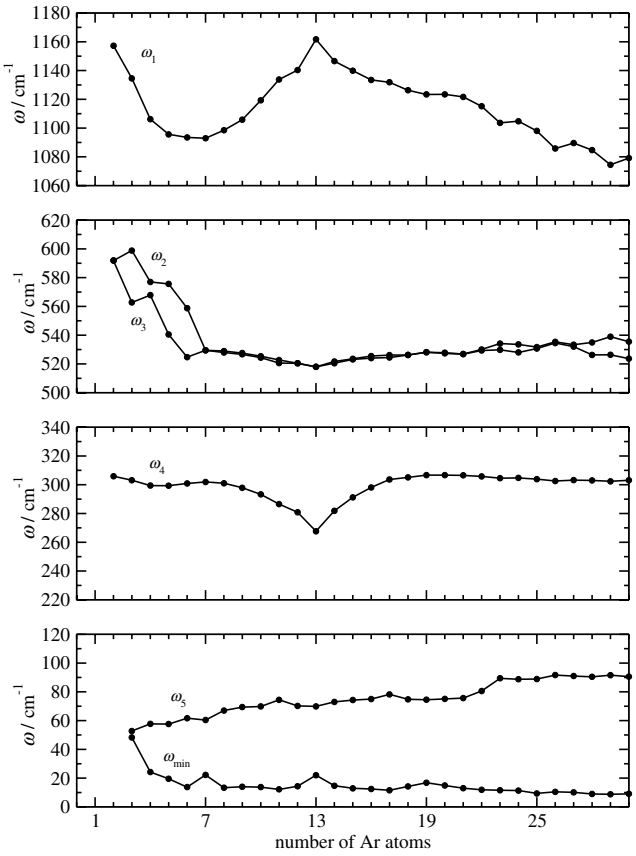

Fig. 6. Graphs of normal frequencies $\omega_i(n)$ of Ar_nH^+ with n = 2–30.

This dependence of the normal frequencies ω_i on n can be qualitatively understood if we take into account the finding (see part I) that the structural and bonding properties of the Ar_2H^+ core fragment do not vary significantly with cluster size n. Most of the effects observed above can then be attributed to the changing mass distribution in the building-up steps. If we take, e.g., for the clusters with n = 2–7 an effective 3-particle model (as extensively treated in textbooks like [19]), it is easily seen that ω_1, ω_2, and ω_3 must become smaller with increasing n, whereas ω_4 should remain roughly unchanged. Since these regularities are so intimately connected with the structural properties of the clusters, it should be possible to set up an increment scheme for the vibrational frequencies, just as was done for the binding energy of the clusters in part I [3]. We shall not embark on this here in more detail.

We conclude this discussion with an illustration of the appearance of the eigenvectors of the normal vibrations. Figure 7 shows the displacement vectors of the atoms in Ar_3H^+ corresponding to the eigenvectors of the six normal vibrations, reflecting clearly their character.

Now we turn to the study of the classical intra-cluster dynamics by multi-dimensional trajectories and the corresponding Fourier spectrum of the nuclear coordinates as functions of time. In Figures 8 and 9 the spectra of Ar_3H^+ and Ar_7H^+, respectively, are shown, each for two different

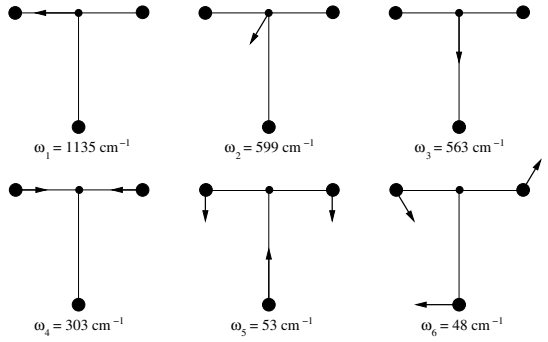

Fig. 7. Normal vibrations of the Ar_3H^+ complex in its most stable structure: frequencies and displacement vectors.

amounts of vibrational energy in the normal modes of the most stable structure; these spectra are to be compared with those for Ar_2H^+ in Figure 3. The following observations are made: (i) For the low-energy vibration ($\nu_i = -0.499$) the spectrum is, apart from the bending frequency splitting in Ar_3H^+ and the appearance of the additional low-frequency lines, largely similar to that for Ar_2H^+, with sharp peaks. (ii) As already seen in the Ar_2H^+ case, the spectrum gets noisy rather quickly when the vibrational energy increases. Also in the larger clusters (we do not give here a full set of spectra but are satisfied with the two examples), the classical motion is predominantly chaotic, even for zero-point vibrational energies, as illustrated by the lower parts of the spectra in Figures 8 and 9. (iii) On adding more Ar atoms, weakly bound to the core fragment, the number of "soft", *anharmonic* modes increases. Notwithstanding the fact that the coupling between two modes may be of quite different strength in each case (e.g., strong between two core modes but weak between Ar wrapper atom vibrations and core vibrations), the total effect of mode coupling is enhanced, and the spectrum gets noisier. This means that enlarging the cluster size leads to an increasing tendency to irregularity in the vibrational motion of such aggregates, as expected.

The general observation is that the chaotic character of the classical intra-cluster dynamics becomes more and more dominant as the internal (vibrational) energy and the cluster size increase. One may speculate about some parallelism to be expected in the quantum dynamics, but such studies are even nowadays still severely hampered by the difficulties in performing sufficiently reliable quantum-mechanical calculations for polyatomic systems (*vide supra*).

4.3 Stability and internal rearrangement processes

To begin with, we return again to the problem of stability of the protonated argon clusters, taking into account the vibrational motions of the atoms in the cluster. In order to make the discussion as clear as possible we consider the relatively simple case of Ar_3H^+ as a prototype example. Figure 10 shows a pictorial representation of relevant geometrical arrangements (stationary points of the PES) and

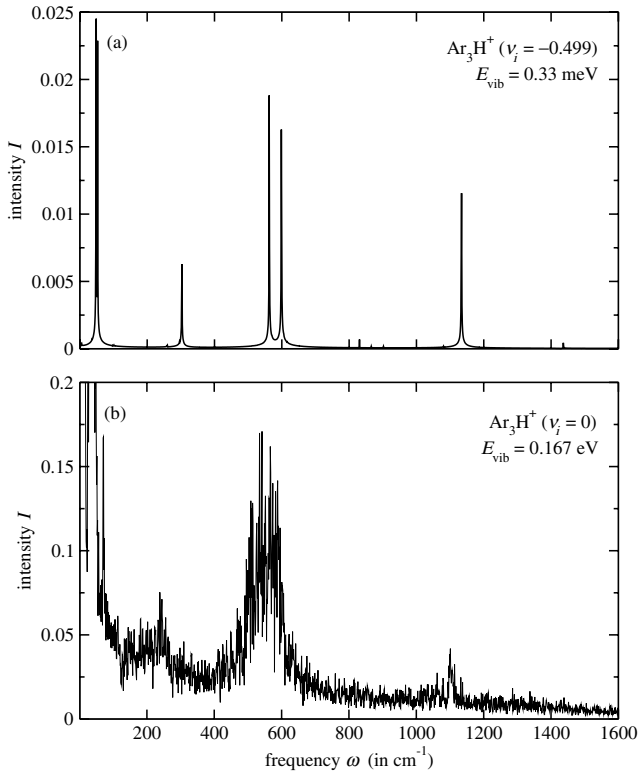

Fig. 8. Fourier spectrum of the superposition of all Cartesian coordinates for classical vibrational motion of the Ar_3H^+ complex in its most stable structure; initial conditions corresponding to normal-mode vibrations: (a) $\nu_i = -0.499$; (b) $\nu_i = 0$.

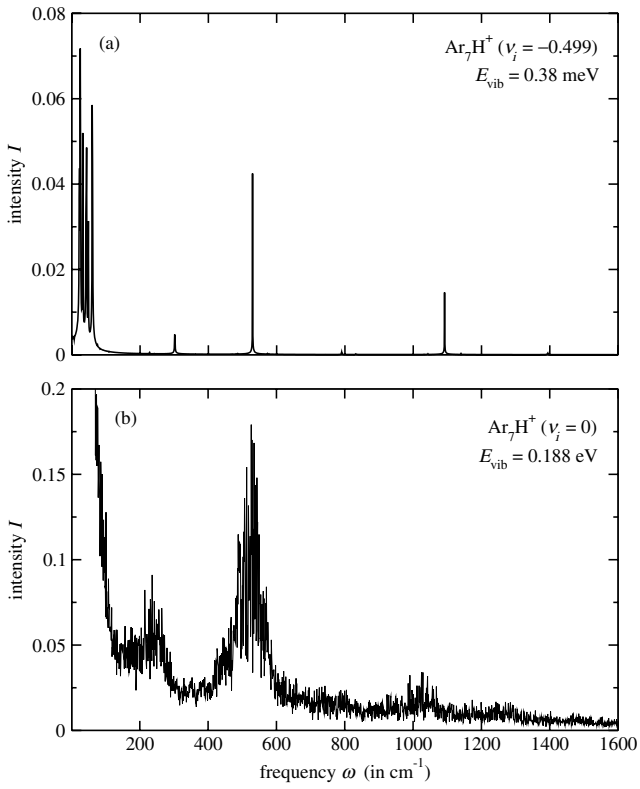

Fig. 9. Fourier spectrum, analogous to Figure 8, for Ar_7H^+: (a) $\nu_i = -0.499$; (b) $\nu_i = 0$.

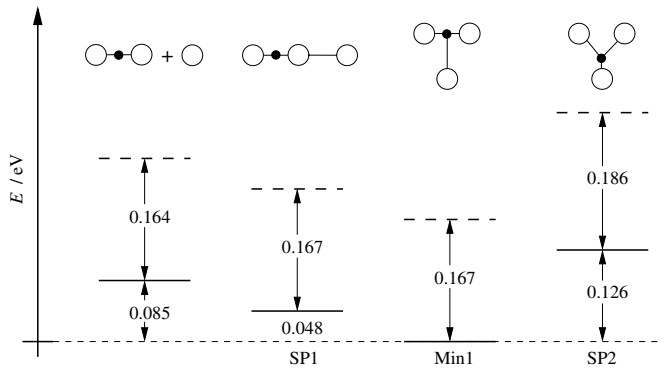

Fig. 10. Geometric structures and energy level diagrams for stationary points on the rearrangement and fragmentation reaction pathways of Ar_3H^+ as obtained in the DIM treatment (in eV, relative to the binding energy E_B of Ar_3H^+). Solid bars: electronic energy; dashed bars: electronic plus zero-point vibrational energy (in harmonic approximation).

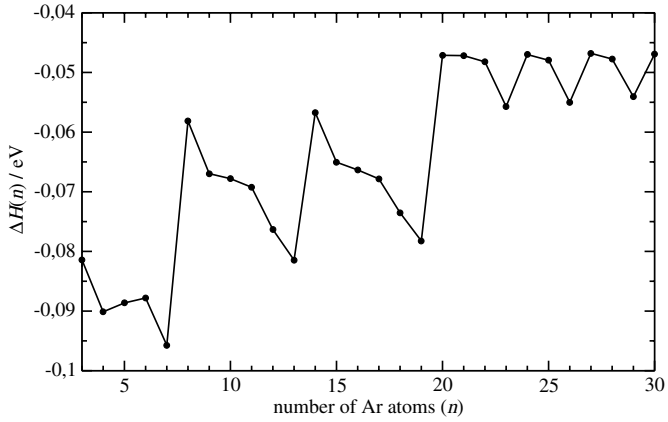

Fig. 11. Graph of the evaporation energy $\Delta H(n)$ of the most weakly bond outer Ar atom in Ar_nH^+ clusters, as defined by equation (7).

corresponding energies with and without the zero-point energy (ZPE) contributions in the harmonic approximation.

The first striking observation from the left side of the diagram in Figure 10 is that the cluster in its global-minimum structure (Min1) is stable against fragmentation (detachment of the outer Ar atom), but only by 82 meV (the difference of E_B + ZPE between Ar_3H^+ and Ar_2H^+). This means that even an excitation of the asymmetric stretch mode of the core fragment of Ar_3H^+ by one quantum (141 meV) provides sufficient energy to split off the outer Ar atom; evidently mode 5 is active in this process (see Fig. 7). For the larger clusters, the stability properties are similar to the Ar_3H^+ case, as can be realized from Figure 11, which shows a graph of the energy required for evaporation of the most weakly bound outer Ar atom in Ar_nH^+ clusters, in dependence on the cluster size (n),

$$\Delta H(n) = \Delta E(n) + \Delta\mathrm{ZPE}(n), \qquad (7)$$

where $\Delta E(n) = E_B(n) - E_B(n-1)$ is the electronic binding energy of the last added Ar atom, defined by equations (2) and (3) in paper I, and $\Delta\mathrm{ZPE}(n) = \mathrm{ZPE}(n) - \mathrm{ZPE}(n-1)$ denotes the additional amount of zero-point energy when attaching an Ar atom to the cluster $Ar_{n-1}H^+$ (all clusters taken in their electronically most stable structure). The medium-sized clusters for the range of n considered here are stable against Ar-atom evaporation with $|\Delta H|$ values between 50 and 90 meV. As in the Ar_3H^+ case, an amount of energy as small as one quantum of the asymmetric stretch vibration of the Ar_2H^+ core fragment (for the larger clusters even a one-quantum excitation of the bending vibration) is sufficient for making the detachment of one of the outermost Ar atoms energetically feasible.

Let us now turn to the intra-cluster atomic migration processes; again we consider in some detail the simple Ar_3H^+ case. From Figure 10 we see that there are two pathways for rearranging the most stable triangular Ar_3H^+ configuration corresponding to Min1. The first route, energetically preferred and connected with vibrational mode 6, is Ar-atom migration via a linear ($C_{\infty v}$) transition configuration (SP1) leading to another triangular arrangement, identical to the starting configuration. The second route, with a higher potential-energy barrier and connected with vibrational mode 3, is proton migration proceeding via a triangular (C_{2v}) transition configuration (SP2).

For gaining at least a qualitative insight into the detailed intra-cluster dynamics, the simplest access is provided by the classical trajectory approach, which will be used in the following discussion. We have to keep in mind, however, that this is a model, not the full truth, and we cannot prove the extent to which the results are realistic. In particular, to which extent quantum effects will modify the picture remains an open question.

In Figure 12 the intra-cluster rearrangement processes are illustrated by a typical classical trajectory representation of the motions of the nuclei for initial conditions of zero-point vibrational energy in each of the normal modes. As can be seen from Figure 10, under these energetic conditions both of the intra-cluster rearrangement channels are open in a classical approach while they are closed in a quantum-mechanical treatment. In the case considered here (i.e., for the specific set of initial conditions chosen), after about 1 ps (Fig. 12b) the proton is the first to change its position, even though the energy barrier to be surmounted is the highest. The transition "jump" itself requires only about 0.15 ps. The positional change of the proton is accompanied by a slightly delayed relaxational motion of the Ar atoms due to the fact that the equilibrium Ar$\cdots$Ar distance in the Ar–H–Ar core fragment is about 1 a_0 shorter than each of the two other Ar$\cdots$Ar distances (5.5 a_0 vs. 6.6 a_0). Thereby the momenta of the Ar atoms increase, which corresponds to some energy transfer into the modes 4, 5, and 6 (note the larger displacement amplitudes of the Ar atoms in Fig. 12b compared with those in Fig. 12a). At t = 1.6 ps (Fig. 12c) there is sufficient energy (and momentum) in mode 6 for starting an internal rotational motion of the $ArHAr^+$ fragment

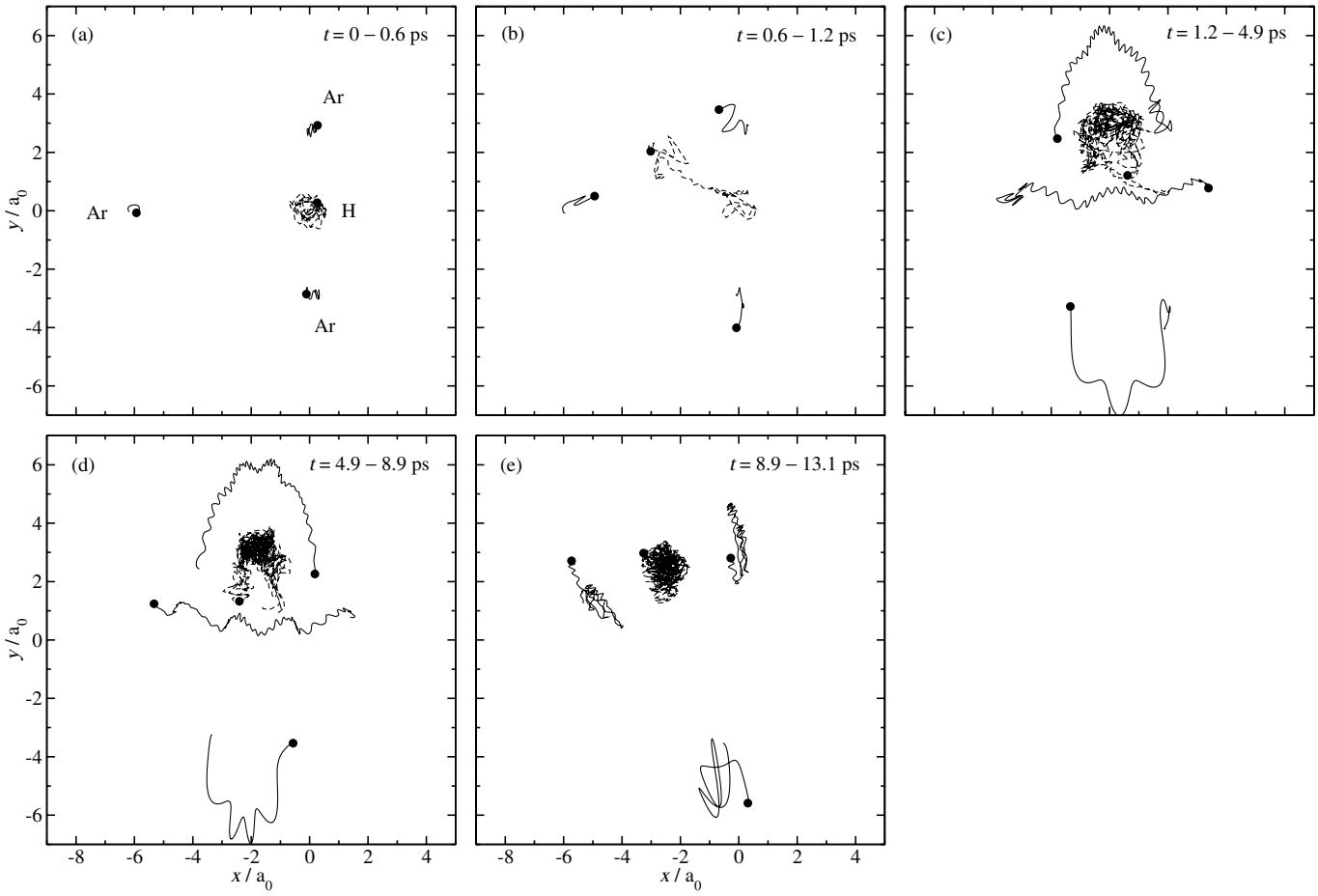

Fig. 12. Intra-cluster rearrangement processes in Ar_3H^+: classical nuclear trajectories for initial conditions of zero-point energy in each of the normal vibrational modes shown in five time windows. To facilitate the orientation, the terminal points of the particle trajectories at the end of each time window are marked with a dot.

against the third Ar atom, or in other words: starting the migration process of the third Ar atom through the linear transition configuration (SP1 in Fig. 10) as mentioned above, leading to another, equivalent triangular arrangement. The whole Ar-atom migration requires 3 ps which is about 20 times longer than for the proton transfer. In Figure 12d the arrangement moves back into its preceding orientation. This is the typical behaviour which we observed in the trajectory studies: once there is sufficient energy in the relevant vibrational modes (here: mode 6), the system flips back and forth while vibrational energy flows off into other modes. This is illustrated by Figure 12e, where mode 6 has lost some part of its energy and the Ar-atom migration process has stopped. Nevertheless there is still a considerable amount of vibrational energy in the modes 4, 5, and 6, which can be seen from the larger amplitudes of the Ar-atom trajectories compared to the elongations in Figure 12a.

For the energies in the case considered here, the Ar-atom evaporation channel is also open in the classical approach (comp. Fig. 10). It is a very slow process which, once initiated, shows no interesting peculiarities; therefore we omit special illustration and discussion.

The findings discussed here show clearly that the internal dynamics of the clusters cannot be understood by considering the energetic aspects alone. It must be taken into account that for initiating one of the competing processes, a sufficiently large amount of energy must flow into the respective active mode. Furthermore, in the present case the processes involve, above all, the motion of either heavy particles (Ar) as in Ar-atom migration and evaporation, or a light particle (H) as in proton migration, whereby the Ar-atom processes are slow while proton migration is fast. This altogether explains qualitatively the observations revealed when running a batch of classical trajectories of the kind characterized above: (i) First of all proton migration takes place; Ar-atom migration and evaporation set in later. Although this seems to contradict the energetic requirements (*vide supra*), it is easily understood from the fact that, as soon as the active mode 3 has acquired sufficient energy (from coupling with other relatively energy-rich core modes), the proton immediately undergoes displacement, whereas for the Ar-atom processes the active modes 5 and 6, which are weakly coupled to the energy-rich core modes, need on the average more time to acquire energy and are much slower so that

energy may partly drain off again. (ii) Proton hopping leads to a certain excitation of accompanying outer-Ar-atom vibrations, which are favourable for subsequent Ar migration.

For larger clusters, the energetics shows a quite analogous situation. The least energy (some 10 meV) is required for outer-Ar-atom (Ar solvent wrapper, so to say) rearrangement, Ar-atom evaporation needs somewhat more energy (50–90 meV), and the largest energy amount (100–200 meV) is necessary for changing the position of the proton between one pair of Ar atoms and another. This means that with only the zero-point energy in each of the vibrational modes all three intra-cluster rearrangement channels are open in the classical approach, and there is a competition between them. Even without performing extended classical trajectory studies, we would expect from the structural and dynamical regularities alone (see Sect. 4.2 and part I) strong analogies to the Ar_3H^+ prototype for the classical rearrangement dynamics of the medium-sized clusters. Thus, supposing again initial conditions with zero-point energy in each of the normal vibrational modes, proton migration should be dynamically preferred (despite the energetic handicap). One would expect not only the sequence of the events (proton migration – Ar-atom migration – Ar-atom evaporation), but also the other aspects of classical intra-cluster dynamics to be basically similar to those in Ar_3H^+.

If we go to higher internal (vibrational) energies, the situation becomes less transparent but the same mechanisms should be effective, at least as long the normal-mode approximation is meaningful.

4.4 UV photodissociation

Clusters with a well-defined chromophore unit could in principle be interesting subjects for studies of energy redistribution and rearrangement in electronically excited polyatomic aggregates. Unfortunately, in the case of protonated argon clusters such processes are overshadowed by fragmentation. As already explained in some detail in part I (see Sects. 3.2.2 and 3.3.2 therein), all low-lying excited electronic states of the Ar_2H^+ core fragment, up to around 10–12 eV above the ground state, are globally repulsive; no stable arrangement of the atomic constituents of the Ar_nH^+ clusters will be formed in the electronic states of the energy range considered. This means that after exciting a cluster Ar_nH^+ vertically from the electronically most stable ground-state structure, it ends up with an energy significantly higher than the asymptotic atomization limit of the set of excited states concerned, namely $(n-1)\mathrm{Ar}(^1\mathrm{S}) + \mathrm{Ar}^+(^2\mathrm{P}^\circ) + \mathrm{H}(^2\mathrm{S})$, and consequently the dominant process following photoexcitation of the cluster is the complete fragmentation into its atomic constituents as indicated above. It cannot be entirely excluded but it appears rather unprobable that (maybe as a result of some secondary processes) any smaller clusters will occur. Because of this situation, the detailed dynamics of the UV photodissociation processes seems less interesting; it has not been pursued further in the present study.

4.5 Collision processes

As envisaged in Section 2, we discuss here some types of collision processes involving protonated argon clusters, namely collisions of a proton or a small Ar_nH^+ complex ($n = 1$ or 2) with a neutral pure Ar_m cluster, according to equations (1) and (2), respectively. It was already mentioned that we intend neither to explore the full variety of possible elementary processes in such systems, nor to make quantitative predictions for cross-sections or rate constants. Therefore, we restricted this part of the study to a system of seven argon atoms and one proton, and we selected only a few out of the many conceivable collision processes in order to visualize some typical elementary events which may happen to the kind of clusters considered here. With this in mind we have run sample trajectories (several tens to hundreds) with appropriately selected initial conditions, for each of the processes considered. The findings are briefly reported in the following paragraphs.

Because of the large exothermicity, the outcome of the type 1 collisions was more or less what one would imagine. Let us consider a very slow proton (say, with kinetic energy below 1 μeV) impinging on an Ar_7 cluster. Compared with the binding (atomization) energy of the cluster (roughly 0.2 eV in the present case), such (relative) translational energy is small. However, because of the attracting polarization forces the proton is accelerated and, most importantly, has the chance to bind strongly to one (or two) of the Ar atoms, thereby releasing a large amount of energy, more than 4 eV. This leads to an "explosion" of the cluster, i.e. to nearly complete fragmentation:

$$\mathrm{H}^+ + \mathrm{Ar}_7 \rightarrow \mathrm{ArH}^+ + 6\mathrm{Ar}\ , \tag{8}$$

or to fragmentation into several small complexes, with a few atoms each. Besides this *direct* process, the fragmentation can also proceed stepwise:

$$\mathrm{H}^+ + \mathrm{Ar}_7 \rightarrow (\mathrm{Ar}_2\mathrm{H}^+)^* + 5\mathrm{Ar} \rightarrow \mathrm{ArH}^+ + 6\mathrm{Ar}\ . \tag{9}$$

Here, the proton first hits the Ar_7 cluster, becoming attached to two of the Ar atoms thus forming a strongly vibrating and rotating transient Ar_2H^+ complex. Finally (after a few ps), this cluster dissociates into ArH^+ and an Ar atom. The rest of the original cluster decomposes in the early stage of the process. For larger clusters, the collision with the proton will be more localized, so that with increasing probability, the collision should also lead to one or more smaller neutral Ar clusters.

It is an interesting question to ask what will happen to an ArH^+ ion produced in the foregoing proton-cluster collision if it meets another neutral argon cluster, for example Ar_6. One possibility is the formation of Ar_2H^+ with atomization of the rest of the neutral cluster by the excess energy of about 0.5 eV, even for very low collision energy, according to

$$\mathrm{ArH}^+ + \mathrm{Ar}_6 \rightarrow \mathrm{Ar}_2\mathrm{H}^+ + 5\mathrm{Ar}\ . \tag{10}$$

For sufficiently slow collisions, larger cluster ions may also form via similar processes:

$$\mathrm{Ar}_2\mathrm{H}^+ + \mathrm{Ar}_5 \rightarrow \mathrm{Ar}_3\mathrm{H}^+ + 4\mathrm{Ar}\ . \tag{11}$$

On the other hand, if we consider collisions of a single Ar atom with a protonated argon cluster, say Ar_6H^+, there should be a chance for simple attachment of an ultra-slow Ar atom leading to a vibrationally and rotationally excited product cluster. The dominant process, however, was found to be the exchange of the incoming argon atom with one from the cluster according to

$$Ar' + Ar_6H^+ \rightarrow Ar_5Ar'H^+ + Ar\ . \qquad (12)$$

The existence of these processes can be taken as a hint to possible routes for the actual generation of Ar_nH^+ clusters, started by the production of ArH^+ molecular ions according to equation (8). This initial step is then followed by the successive formation of larger ionic complexes in processes like equations (10) and (11).

5 Summary and conclusions

In this second part of our study we exploit the tools provided in the first part for generating, in a very efficient way, potential-energy surface data for protonated argon clusters, to investigate the dynamics of such systems, making use also of our knowledge about the bonding and structural properties. The focus of our effort is on gaining information about the intra-cluster motions, in particular the vibrations, and the question of regularity vs. irregularity in dependence on the cluster size. Except for the simple triatomic fragment Ar_2H^+, for which we are able to calculate accurate quantum states of vibration, we rely for the larger systems on the normal-mode and the classical trajectory approaches. In addition to nonreactive dynamics we explore also, for the small cluster with $n = 3$, the intra-cluster rearrangements (proton and Ar-atom migration), including also Ar-atom detachment. Finally some illustrative findings are presented for possible collision processes involving protonated argon clusters, obtained likewise in a classical trajectory treatment.

The main results are the following.

1. The minimum-basis-set diatomics-in-molecules (DIM) approach with ab-initio input data proved to be a sufficiently reliable tool for generating the interaction potential-energy data necessary in studies of the dynamics of polyatomic systems like the protonated argon clusters. The method is so efficient that each potential-energy value can be calculated at the moment it is needed, e.g. "on the fly" in a classical treatment of a collision.
2. For the non-rotating triatomic fragment Ar_2H^+ ($J = 0$) the quantum states of vibration have been accurately determined using an improved filter diagonalization method. This was done in order to cross-check the results of the normal-mode approach and to investigate the question of quantum irregularity in these systems. Whereas the zero-point energy is very accurately reproduced in the harmonic approximation, the vibrational energy level spacings show the expected deviations from the quanta obtained in the harmonic approximation. No indication of "quantum chaos" is found.
3. The classical internal dynamics of Ar_2H^+ as reflected in the Fourier spectra of dynamical variables (here: coordinates) as functions of time shows characteristics analogous to earlier findings for systems of this kind: a clean line spectrum for very low energies (far below zero-point energy in the present case) followed by an early onset of irregularity (classical chaos) as energy increases. This is a consequence of anharmonicity and mode coupling in the potential energy.
4. The normal frequencies of the clusters Ar_nH^+ with $n > 2$ can be grouped into subsets: the four largest frequencies are attributed to the vibrations of the linear inner Ar_2H^+ fragment (asymmetric stretch, twofold bending, symmetric stretch); the remaining (low) frequencies belong to vibrations of the outer attached Ar atoms. The n-dependency of the Ar_2H^+ fragment frequencies exhibits characteristic features which are clearly related to the building-up sequence discussed in part I (reflecting, for example, magic numbers), whereas the low frequencies form a band spreading between a few cm^{-1} and about 100 cm^{-1}.
5. The classical internal dynamics of the clusters Ar_nH^+ with $n > 2$ shows an increasing degree of irregularity with increasing energy (like that exhibited in many triatomic cases) and cluster size (n).
6. All clusters Ar_nH^+ (as mentioned in part I) are not only electronically stable but remain so also with inclusion of the zero-point vibrational energy. Even a little vibrational excitation, however, causes internal rearrangement processes. Proton migration turns out to be dynamically preferred (despite the energetic handicap) over Ar-atom migration and evaporation.
7. As already discussed in part I, electronic (UV/visible light) excitation always leads to fragmentation (up to atomization) of the clusters because of the globally repulsive nature of the excited-state potential-energy surfaces in the energy range below about 10 eV.
8. Out of the various conceivable collision processes involving protonated argon clusters, a few selected processes are discussed here, which could be illustrative examples of those playing a role in the gas-phase formation of medium-sized clusters Ar_nH^+, started by proton collisions with neutral Ar_m clusters. For this study the classical trajectory approach has been applied. The examples are restricted to the case of one proton and seven argon atoms, but presumably the findings can be generalized.

In conclusion, we may state, that our relatively crude "minimal ab-initio DIM model" for generating the PES data allows a successful treatment not only of the structure but also of the dynamics of medium-sized Ar_nH^+ clusters. This fact is encouraging for an extension of the investigations to more complicated systems. Work in this direction is in progress.

The authors thank the referees for several useful comments and suggestions.

References

1. T.A. Miller, V.E. Bondybey, *Molecular Ions: Spectroscopy, Structure, and Chemistry* (North-Holland, New York, 1983)
2. *Clusters of Atomcs and Molecules*, edited by H. Haberlandt (Springer-Verlag, Berlin, 1994), Vols. I and II
3. T. Ritschel, P.J. Kuntz, L. Zülicke, Eur. Phys. J. D **33**, 421 (2005); part I of this series
4. F. Ragnetti, Ch. Zuhrt, L. Zülicke, in *Femtochemistry*, edited by M. Chergui (World Scientific Publ. Comp., Singapore, 1996)
5. L. Zülicke, F. Ragnetti, R. Neumann, Ch. Zuhrt, Int. J. Quant. Chem. **64**, 211 (1997)
6. Ch. Zuhrt, R. Neumann, L. Zülicke, Chem. Phys. **240**, 117 (1999)
7. L. Zülicke, R. Neumann, Ch. Zuhrt, J. Schretter, Int. J. Quant. Chem. **80**, 486 (2000)
8. *Reaction Dynamics in Clusters and Condensed Phase*, edited by J. Jortner, R.D. Levine, P. Pullman (Kluwer Academic Publishers, Dordrecht, 1994)
9. (a) D. Neuhauser, J. Chem. Phys. **93**, 2611 (1990); D. Neuhauser, J. Chem. Phys. **100**, 5076 (1994); (b) V.A. Mandelshtam, T.P. Grozdanov, H.S. Taylor, J. Chem. Phys. **103**, 10074 (1995); (c) V.A. Mandelshtam, H.S. Taylor, J. Chem. Phys. **106**, 5085 (1997)
10. T. Ritschel, L. Zülicke, P.J. Kuntz, Z. Phys. Chem. **218**, 377 (2004)
11. MOLPRO is a package of ab initio programs written by H.-J. Werner and P.J. Knowles, with contributions from R.D. Amos, A. Bernhardsson, A. Berning, P. Celani, D.L. Cooper, M.J.O. Deegan, A.J. Dobbyn, F. Eckert, C. Hampel, G. Hetzer, T. Korona, R. Lindh, A.W. Lloyd, S.J. McNicholas, F.R. Manby, W. Meyer, M.E. Mura, A. Nicklass, P. Palmieri, R. Pitzer, G. Rauhut, M. Schütz, H. Stoll, A.J. Stone, R. Tarroni, T. Thorsteinsson
12. D.E. Woon, T.H. Dunning Jr, J. Chem. Phys. **99**, 3739 (1993)
13. P.J. Kuntz, J.L. Schreiber, J. Chem. Phys. **76**, 4120 (1982)
14. L. Zülicke, Ch. Zuhrt, X. Chapuisat, C. Saint-Espès, Int. J. Quant. Chem. **52**, 227 (1994)
15. (a) Z. Bačić, J.C. Light, Annu. Rev. Phys. Chem. **40**, 469 (1989); (b) J.C. Light, T. Carrington Jr, Adv. Chem. Phys. **114**, 263 (2000)
16. R. Radau, Ann. Sci. ENS **5**, 311 (1868)
17. D.T. Colbert, W.H. Miller, J. Chem. Phys. **96**, 1982 (1992)
18. Ch. Zuhrt, to be published
19. G. Herzberg, *Molecular Spectra and Molecular Structure. II. Infrared and Raman Spectra of Polyatomic Molecules* (D. van Nostrand Comp., New York, 1964)
20. M.D. Pattengill, *Classical Trajectory Methods*, in: *Atom-Molecule Collision Theory*, edited by R.B. Bernstein (Plenum Press, New York, 1979)
21. (a) D.L. Bunker, Methods Comp. Phys. **10**, 287 (1971); (b) L.F. Shampine, M.K. Gordon, *Computer Solution of Ordinary Differential Equations* (W.H. Freeman and Comp., San Francisco, 1975)
22. R. Car, M. Parrinello, Phys. Rev. Lett. **55**, 2471 (1985) and later articles
23. J.Y. Qu, W. Li, R. Guo, X.S. Zhao, J. Chem. Phys. **117**, 2592 (2002)